BOLETIN DE LA SOCIEDAD ESPAÑOLA DE
Cerámica y Vidrio
www.elsevier.es/bsecv

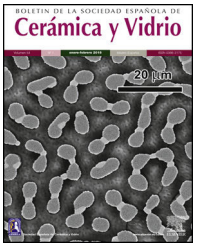

The effect of Ag incorporation on the characteristics of the polymer derived bioactive silicate phosphate glass-ceramic scaffolds

Amirhosein Paryab[a], *Toktam Godary*[a], *Rashid Khalilifard*[a], *Adrine Malek Khachatourian*[a,*], *Farnoosh Abdollahi*[b], *Sorosh Abdollahi*[c]

[a] *Department of Materials Science and Engineering, Sharif University of technology, Tehran, Iran*
[b] *Department of Dentistry, Kashan University of Medical Science, Kashan, Iran*
[c] *School of Metallurgy and Materials Engineering, Iran University of Science and Technology, Tehran, Iran*

ARTICLE INFO

Article history:
Received 24 March 2021
Accepted 22 June 2021
Available online 8 July 2021

Keywords:
Polymer derived ceramics
Glass-ceramics
Scaffolds
Bioactivity
Silver incorporation
Antibacterial activity

ABSTRACT

In the bone tissue engineering field (BTE), it is of significant importance to develop bioactive multifunctional scaffolds with enhanced osteoconductivity, osteoinductivity, and antibacterial properties required for lost bone tissue regeneration. In this work, a bioactive glass-ceramic scaffold was manufactured via a novel polymer-derived ceramics (PDC) manufacturing method. To gain antibacterial properties, the silver ions were incorporated in controlled amount along with other precursors in the PDC processing stage. Microstructural and structural properties of the fabricated silicate-phosphate glass-ceramic scaffold were evaluated by scanning electron microscopy (SEM) equipped with energy dispersive spectroscopy (EDS) and X-ray diffraction (XRD) analysis, respectively. Furthermore, bioactivity, antibacterial, and cytotoxicity evaluation of PDC scaffolds were conducted. The microstructural analysis determined that scaffolds have interconnected porous network with two different pore range size favorable for osteointegration and bone formation. The structural analysis confirmed that fabricated glass-ceramic scaffolds contain bioactive octacalcium phosphate (OCP) phase responsible for enhanced bioactivity and HCA formation during the immersing of scaffolds in simulated body fluid (SBF) for several days. Moreover, PDC scaffolds with Ag nanoparticles showed considerable antibacterial properties against Gram-negative Klebsiella pneumoniae and Gram-positive Staphylococcus aureus bacteria cells. This study has demonstrated that it is possible to develop a novel group of antibacterial and bioactive Ag incorporated silicate-phosphate glass-ceramic scaffolds for BTE applications, such that, it was verified in vivo.

* *Corresponding author.*
E-mail address: khachatourian@sharif.edu (A. Malek Khachatourian).
https://doi.org/10.1016/j.bsecv.2021.06.005

El efecto de la incorporación de Ag en las características de los andamios de vitrocerámica de fosfato de silicato bioactivo derivado de polímeros

Palabras clave:
Cerámica derivada de polímeros
vitrocerámica
Andamios
Bioactividad
Incorporación de plata
Actividad antibacterial

R E S U M E N

En el campo de la ingeniería de tejido óseo (BTE), es de gran importancia desarrollar andamios multifuncionales bioactivos con osteoconductividad mejorada, osteoinductividad y propiedades antibacterianas necesarias para la regeneración del tejido óseo perdido. En este trabajo, se fabricó un andamio de vitrocerámica bioactive mediante un nuevo método de fabricación de cerámica derivada de polímeros (PDC). Para obtener propiedades antibacterianas, los iones de plata se incorporaron en una cantidad controlada junto con otros precursores en la etapa de procesamiento de PDC. Las propiedades microestructurales y estructurales del armazón de cerámica de vidrio de silicato-fosfato fabricado se evaluaron mediante microscopía electrónica de barrido (SEM) equipada con espectroscopía de dispersión de energía (EDS) y análisis de difracción de rayos X (XRD), respectivamente. Además, se llevó a cabo una evaluación de bioactividad, antibacteriana y citotoxicidad de los andamios de PDC. El análisis microestructural determinó que los andamios tienen una red porosa interconectada con dos tamaños de rango de poros diferentes favorables para la osteointegración y la formación de hueso. El análisis estructural confirmó que los andamios de vitrocerámica fabricados contienen una fase de fosfato octacálcico bioactivo (OCP) responsable de la bioactividad mejorada y la formación de HA durante la inmersión de los andamios en fluido corporal simulado (SBF) durante varios días. Además, los andamios de PDC con nanopartículas de Ag mostraron considerable propiedades antibacterianas contra las células de bacterias Gram-negativas Klebsiella pneumoniae y Gram-positivas Staphylococcus aureus. Este estudio ha demostrado que es posible desarrollar un grupo novedoso de andamios de vitrocerámica de silicato-fosfato incorporados en Ag antibacterianos y bioactivos para aplicaciones de BTE, de manera que se verificó in vivo.

Introduction

Annually four million surgical operations are being conducted for bone graft and other healing processes to prevent the problems caused by trauma or congenital reasons [1]. However, such treatments face significant limitations since autograft and allograft suffer from size limitations of transplanting organs and the risk of disease transmission. Furthermore, metal transplants carry the risk of revision surgery and stress shielding [2]. In order to overcome these limitations, widespread research is being carried out in bone tissue engineering (BTE) to design and manufacture specific porous structures mimicking the cancellous texture of native extra cellular matrix (ECM). It is worth mentioning that such native ECM is secreted by Fibroblast in the organ while via using an appropriate biodegradable scaffold, the attaching of mentioned cells is facilitated and the resolved parts of the scaffold are substituted by secreted ECM structure [3]. Scaffolds used in BTE have to be bioactive to bind to the surrounding bone tissue and contain open and interconnected pores to provide bone cell ingrowth (osteoconduction) and cause osteogenic cells to differentiate into bone cells (osteoinduction) [4].

In general, a scaffold is a biocompatible, biodegradable, 3D porous material capable of supplying necessary load-bearing and degrading at a specific rate so the host tissue could replace the scaffold obviating the subsequent surgery to remove the material. Moreover, the scaffold must provide cell attachment and proliferation [5]. Scaffold pore size and density are critical issues in the scaffolds design for BTE applications. It was shown that BTE's scaffolds need to be composed of a range of pore sizes. Macropores (>300 μm) assist osteogenesis since they have high permeability and potential for angiogenesis and vascularization. On the other hand, pores less than 10 μm (micropores) help cell-scaffold interaction and develop osteogenic effects [6]. However, the interconnection of porosities with different sizes is an absolute necessity; firstly, because of cell infiltration after cell seeding caused by capillary forces, and secondly, because of the importance of transportation of nutrients and oxygen, and waste removal [3]. In order for an osteo-scaffold to successfully replicate the bone mechanobiology behavior it must have an elastic modulus between 10 and 30 GPa and compressive strength of between 100 and 200 MPa [7].

Bioactive glasses (BGs) are mainly produced via melt-casting [8] and sol–gel [9] methods that have been extensively used in BTE applications. They could bond to the surrounding bone tissue since a layer of hydroxy carbonated apatite (HCA) is formed on their surface when contacted by physiological fluids. It was also shown that ions released from BGs facilitate bone formation via activating growth factors and eliciting intracellular and extracellular responses [10]. Despite their promising properties, they suffer from low strength in usage. As a result, bioactive glass-ceramics were introduced with a superior strength in comparison to bioactive glasses; Although it should not be ignored that this strategy

reduced the bioactivity, such that, in all reports lower precipitation of HCA has been evident [11,12]. Nevertheless, some compounds crystalizing inside BGs have been proved to be bioactive like $Na_4Ca_4Si_6O_{18}$, wollastonite, octacalcium phosphate, and apatite [13,14]. Metal and metalloid nanoparticles are employed in different biomedical applications. Among them, silver and silver ions have been traditionally regarded as effective antibacterial agents and widely used by Mediterranean and Asian cultures since ancient times against various infections [15–18]. In recent years researchers are trying to improve the antibacterial activity of scaffolds by different nanoparticles such as Ag, Se, Cu, etc. Vitale-Brovarone et al. [19] incorporated Ag ions inside 3D-glass-ceramic scaffolds through ion exchange to improve antibacterial properties for bone grafting. Wu et al. [20] studied the incorporation of Cu^{2+} ions inside mesoporous bioactive glass (Cu-MBG) scaffolds. The results confirmed that scaffolds have antibacterial properties and hypoxia-like tissue reaction significantly enhanced by Cu^{2+} ions incorporation leading to the coupling of osteogenesis and angiogenesis required for the treatment of bone defects.

Among bioactive glasses and glass-ceramics, silicate-phosphate family is attracting increasing interest among researchers for scaffold formation [21,22]. In the present study, silicate phosphate glass-ceramic scaffolds are manufactured via a unique polymer-derived ceramics (PDC) technique. The synthesis of osteo-scaffolds via PDC method has shown brilliant characteristics, although there are still so many unknown aspects. This approach is commenced with a silicone resin with added micron-sized non-active or active fillers. The whole system can be formed through various methods, including extruding, injecting molding, printing, and ink writing [23]. During heat treatment of the above mixture, the polymer starts to decompose and then reacts with fillers, resulting in an amorphous silicate phase (glass network); this process refers to ceramization [24]. Dissociation of the active fillers and volatilization of the polymer create a considerable portion of interconnected porosity due to the formation and sublimation of gas products leading to the scaffold's formation. Due to the molecular homogeneity of the precursor materials, the glass matrix and the final crystalline phases yield at lower temperatures in the PDC process than conventional melt-casting methods [25–27]. Moreover, the noted manufacturing procedure for glass and glass-ceramic production is much more economical than the sol–gel method that requires expensive precursors [24,28]. The type and amount of crystallized phases in the PDC method can be tuned by the starting materials and heat-treatment procedures. We have already reported that the K_2HPO_4 phosphate salt acts as an efficient P_2O_5 source in PDC scaffolds [29].

In the present study, multifunctional silicate-phosphate glass-ceramic scaffolds are manufactured by the PDC method. To develop multifunctional scaffolds, the effect of silver incorporation in the bioactivity, antibacterial activity, and cytotoxicity of scaffolds is evaluated. First, scaffolds are manufactured by the PDC method, and then the scaffolds' HCA formation behavior in simulated body fluids (SBF) has been assessed. Then, the capacity of the system to accept bactericidal silver material has been addressed, and the bactericidal activity test of the scaffolds was conducted. In the end, the cytotoxicity of materials in contact with osteoblast cells was investigated.

Table 1 – The chemical compositions of the samples.

Materials (wt%)	Sample code		
	6%P(Ag)	6%P	9%P
Silicone	54.32	54.32	52.78
K_2HPO_4	6	6	9
$Ca(OH)_2$	25.39	25.39	24.67
$MgCO_3$	14.46	14.46	14.05
$AgNO_3$	5 wt% of silicone	0	0

Materials and methods

Materials

Silicone resin (PDMS) with commercial name of room temperature volcanizing (RTV2) and a 56.6 wt% of ceramic yield with an appropriate hardener was used in this study. Other raw materials listed here were all purchased from Merck and the solid powders were passed through 400 sieve size: 2-propanol (C_3H_8O), trisaminomethane ($NH_2C(CH_2OH)_3$), Sodium sulphate (Na_2SO_4) 7757-82-6, calcium chloride dihydrate ($CaCl_2{\cdot}2H2O$), hydrogen chloride solution (HCl), sodium hydrogen phosphate (Na_2HPO_4), sodium hydrogen carbonate ($NaHCO_3$), sodium chloride (NaCl), magnesium chloride hexahydrate ($MgCl_2{\cdot}6H_2O$), magnesium hydroxide ($Mg(OH)_2$), potassium chloride (KCl) 7447-40-7, silver nitrate ($AgNO_3$), calcium carbonate ($CaCO_3$), potassium hydrogen phosphate (K_2HPO4).

Glass-ceramic scaffolds production

PDC technique is used to manufacture silicate-phosphate glass-ceramic scaffolds. The details of the optimum heat treatment procedure have been addressed in our previous research [29]. Typically, 2-propanol and silicone resin were mixed with a 1:1 (wt/wt) ratio. Then, the fillers were added slowly in the solution and stirred for 1 hour. In the last 2 min, the hardener equal to 10 wt% of initial silicone, was added to the mixture. Finally, using a syringe the prepared blend was injected into the aluminum foil cups. After one overnight being at room temperature, the samples were cured for 6 h at 60 °C in an oven. At last, the aluminum foil cups were removed and the samples were heat-treated at 500, 870, and 1000 °C with 30 min soaking time in each temperature (heating rate 5 °C/min, air atmosphere). For 6%P(Ag) sample appropriate amount of $AgNO_3$ previously dissolved in 5 ml ethanol was introduced to the initial mixture of silicone and 2-propanol, and the subsequent steps were the same. Table 1 shows the raw material composition of the silicate-phosphate glass-ceramic scaffolds.

Structural and microstructural analysis

For the structural investigation of the samples, an X-ray diffractometer (XRD, Panalytical-2009, UK) with a lamp of Cu Kα radiation (0.15418 nm) was used. For microstructural

assessments, initially samples were sputter coated by an ultra-thin layer of Au/Pd, then fixed and connected to the conductive holder by the conductive tape. A field emission electron microscopy (FESEM, TeScan Mira III, Czech Republic) equipped with an energy dispersive spectroscopy (EDS detector, Oxford instrument) was employed to visualize the microstructure.

Bioactivity measurement

For the bioactivity evaluation of the fabricated glass-ceramics scaffolds, 0.2 g of each sample was immersed in 5 ml SBF solution for 7, 14, and 21 days. Upon removing them from SBF, they were washed with DI water and acetone. 0.1 g of 6%P and 9%P samples were placed in 1 ml of DI water for 7, 14, and 21 days and the solution was kept for ANOVA evaluation of Ca and Ag ions released in water and was performed using the ICP method (ICP, Varian ICP-OES 730-ES, U.S). FT-IR analysis (Vertex 70 FT-IR spectrometer, Bruker) was used to study the phase evolution on the surface of the samples upon removing them from SBF. The SBF preparation instruction is as follows: 0.6545 g NaCl, 0.2268 g $NaHCO_3$, 0.0373 g KCl and 0.0141 g Na_2HPO_4 was added to the 96 ml of DI water one by one with 3 minutes' intervals under the vigorous stirring. The prepared solution was heated to 37 °C, then 0.0304 g $MgCl_2{\cdot}6H_2O$, 9 ml of 1 M HCl solution, 0.0367 g $CaCl_2{\cdot}2H_2O$, 0.0071 Na_2SO_4, and 0.6057 g Tris were added into the solution in the same fashion above. Finally, 3 ml of 1 M HCl was added and the pH of the solution was measured at 37 °C (pH 7.4).

Antibacterial activity assessment

The antibacterial activities of the 6%P and 6%P(Ag) glass-ceramic scaffolds were evaluated against Gram-negative Klebsiella pneumonia (ATCC 13883) and Gram-positive Staphylococcus aureus (ATCC 25923) bacteria cells. A broth microdilution technique was carried out to indicate minimum inhibitory concentrations (MICs) of materials, the lowest concentration of a material at which the microorganism does not display noticeable growth, according to the Clinical and Laboratory Standards Institute (CLSI 2005). Tests were conducted in Müller Hinton broth. Broth cultures were prepared for each strain overnight, and the final concentration in each well was adjusted to 2×10^6 CFU/ml. The samples were crushed into powder. Then serial doubling of dilutions of samples in 1% dimethylsulfoxide was prepared in a 96-well microtiter plate Müller Hinton broth, over the range of 1000–12.5 μg/ml. As a growth indicator, 0.05% triphenyl tetrazolium chloride (TTC) was added to the culture medium. As a positive control of growth, wells comprising only the microorganisms in the broth were used. Bacteria growth was evaluated after 24 h of incubation at 37 °C. For all MIC determinations two positive growth controls were included and the tests were carried out in duplicate.

Cytotoxicity investigation

In this study, MG-63 cell (NCBI C555) taken from the Pasteur Institute of Iran cell bank was used. The cells were de-freezed and transferred to a flask containing DMEM + F12 culture medium with 10% FBS, then incubated at 37 °C, 90% humidity, and 5% carbon dioxide concentration. It should be noted that the culture medium was refreshed every 3–4 days. The extraction method (ISO 5-10993 standard) was used to determine the chemical toxicity of the scaffolds (due to the released ions) and their effect on cell growth and proliferation. First, the samples were autoclaved to become sterilized. Then 1 ml of culture medium was added to each crushed sample per 0.1 g. Then, after 7, 14, and 21 days, the medium was removed and added to the cells. A certain amount of culture medium (DMEM + F12) was also considered as a control. In order to study the physical toxicity of materials (particularly silver clusters) and the rate of cell proliferation, 10^4 cells with 100 μl of culture medium were poured into each well of a 96-well cell culture plate and then incubated at 37 °C for 24 h to allow the cells to adhere to the plate bottom. Then, the culture medium was removed from the cells as much as possible and 90 μl of the extract of each prepared sample along with 10 μl of FBS was added to each culture well, and the cells were exposed to these extracts for another 24 h. Then the culture medium was removed, and 100 μl of MTT at a concentration of 0.5 mg/ml was poured into each well and incubated for 4 h. After that, the solution was removed from the cells, and isopropanol was added to dissolve the purple crystals. To dissolve the MTT precipitate better, the culture plate was shaken on a shaker for 15 min. Then, the solute concentration in isopropanol was determined using an ELISARIDER device (STAT FAX 2100, USA) at 545 nm wavelength.

In vivo test

Nine female Lewis rats weighing 150–250 g were used for the experiment, anesthetized by injection of ketamine through the peritoneum. An incision was made on the cranium dorsal surface and a dental bur was used to produce the defects, with a size around 4 mm diameter. Then the prepared implants were inserted at the defected sites. The incisions were sutured and animals recovered with sufficient situation, food, and water. Every 5 days until the 15th day, 3 animals were euthanized and the implants were harvested by scratches at the site and kept in the fixative solution to be evaluated histologically.

Cellular visualization

Response to Ca^{2+}

1 ml of culture medium was added to the crushed samples 6%P and 9%P per 0.1 g. After 21 days, the medium was removed and added to the cells, such that, two cell solutions were prepared with cell density equal to 10,000 cell/ml. These were accompanied by a control solution prepared with 1 ml of fresh medium and 10,000 cells. The cell solutions were added to the TCPS well-plate and incubated for two hours at 37 °C, 90% humidity, and 5% carbon dioxide concentration. Then, the morphology of cells was visualized by optical microscopy.

Histological visualization

The harvested implants of rats were retrieved and fixed for 24 h at 48 °C in 10% phosphate buffered formalin. Fixed tissues were bisected through both defects, decalcified in 15% formic acid for 24 h, paraffin-embedded, and sectioned at 6 μm. Then

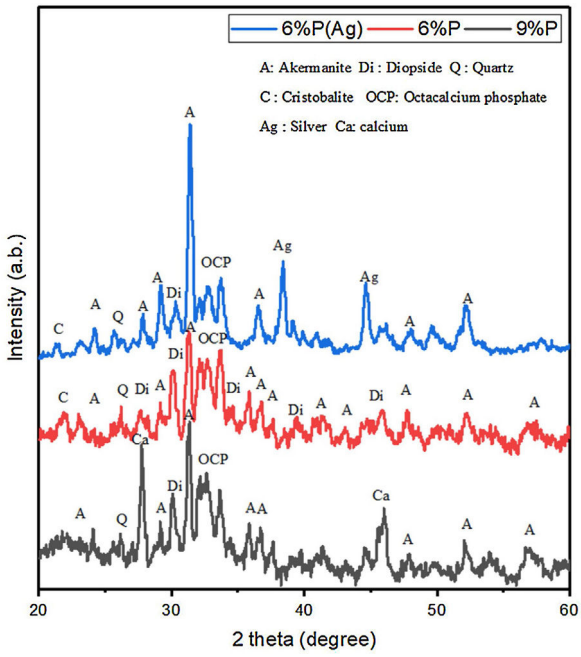

Fig. 1 – XRD spectrum of the 6%P, 6%P(Ag), and 9%P sample heat treated at 1000 °C.

the sections were stained with hematoxylin and eosin (H&E). Sections were imaged using a Hamamatsu NanoZoomer S360 microscope (Japan).

Results and discussion

Structural and microstructural evaluation of PDC scaffolds

Fig. 1 shows the XRD spectrum of the 6%P, 6%P(Ag), and 9% P sample heat-treated at 1000 °C. It can be noted that the scaffolds contain crystalline phases like akermanite, diopside, quartz, cristobalite, and the bioactive octacalcium phosphate (OCP) phase. OCP is known as a suitable precursor for HA or HCA formation required for bone growth. For the 6%P(Ag) sample, it is observed that incorporation of $AgNO_3$ into the 6%P(Ag) mixture and further heat treatment at 1000 °C facilitated the crystallization of metallic silver, whose peaks are detected in the XRD spectrum. It is hypothesized that the reductive atmosphere in the porosities, produced by burn-out of organic moieties at 1000 °C, facilitated the reduction of Ag^+ to Ag^0 in the 6%P(Ag) sample. For the 9%P-1000 °C sample with a higher K_2HPO_4 amount, the metallic calcium precipitation was determined in the XRD spectrum. It is also hypothesized that the burning of organic precursors consumes the oxygen trapped inside the scaffolds porosities and changes the atmosphere to a reductive state appropriate for reducing some Ca^{2+} ions to a metallic state [30].

Fig. 2 shows the FESEM images of the PDC 6%P, 9%P, and 6%P(Ag) scaffolds accompanying their respective EDS elemental analysis of specified points. It is observed that scaffolds have porous microstructure with two different micro and macro-porosities (respectively from 50–500 nm to 50–2000 μm). The smaller porosities are caused by the decomposition of the polymer in the air atmosphere, and the larger ones are caused by gas moieties from the dissociation of active fillers, making their way out of the material. Micrographs show that materials possess a maze structure of interconnected pores ideal for BTE applications. Based on Fig. 2(c), the microstructural assessment showed the precipitation of Ag^0 clusters with sizes of below 1 μm, although the EDS spectrum showed some negligible impurities, except silver. It is confirmed that the PDC method could facilitate the incorporation of Ag^+ ions by introducing active fillers such as $AgNO_3$ into the glass structure. It is worth mentioning that the formation of such Ag nanoparticles is owed to the in situ passive atmosphere, which has been produced inside the bulk

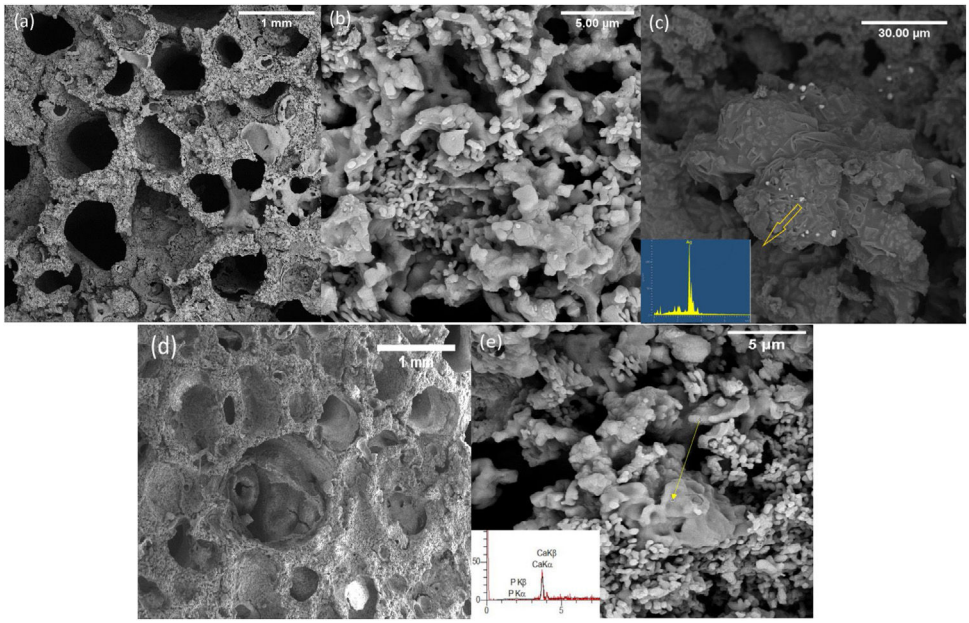

Fig. 2 – FESEM images of (a,b) 6%P, (c) 6%P(Ag), and (d,e) 9%P samples accompanying with their respective EDS analysis.

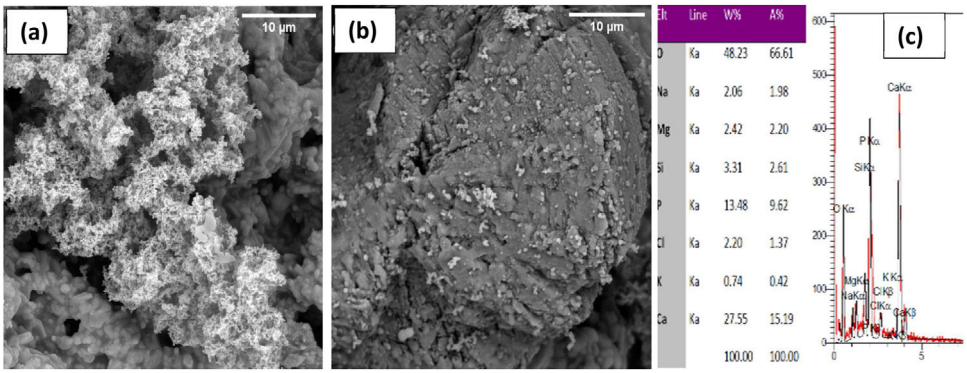

Fig. 3 – (a) HCA formation on the surface of 6%P, (b) poor HCA formation on the surface of 9%P, and (c) the EDX analysis of HCA particles in 6%P.

silicon-containing samples. In fact, thanks to the presence of hydrogen and carbon in the structure of poly-dimethyl siloxane, during the heat treatment, the mentioned elements form gaseous phases of CO, CO_2, H_2, and H_2O. The mentioned gas is escaped from the bulk samples producing micro-porosities. However, due to the maze microstructure of the sample (Fig. 2), it is probable to assume that this gas exhaustion is not done immediately. Thus, such a local passive atmosphere has facilitated the reduction of silver ions. The effect of such a passive atmosphere is obvious even by increase of K_2HPO_4 and in absence of Ag^+, such that, other ions are reduced. According to Fig. 2(e), sample 9%P, metallic calcium clusters are evident, targeted by EDS elemental analysis and in accordance with phase analysis (Fig. 1). It means that in this case, Ca^{2+} has been reduced to Ca^0.

Bioactivity, antibacterial and cytotoxicity evaluation of PDC scaffolds

Fig. 3 shows the FESEM images of the 6%P and 9%P samples immersed in SBF solution for 14 days. According to Fig. 3(a) which is related to the 6%P sample an area with different contrast and texture is evident on the surface of the scaffold ascribed to hydroxyapatite (HA) or Hydroxy carbonated apatite (HCA). Thus, 6%P sample showed significant bioactivity. Further analysis through EDX elemental spectroscopy (Fig. 3(c)) revealed a calcium phosphate phase whose Ca:P ratio is nearly 1.57 which is near the theoretical ratio of the Ca:P in HA. HCA formation is owing to the dissolution of the OCP phase or its hydrolysis to HA. Unlike the 6%P sample, which showed bioactivity, the 9%P sample showed negligible HCA formation on its surface making it hardly bioactive (Fig. 3(b)). Here, one can ask the Ca:P ratio of HCA is 1.66; it is worth mentioning, the Ca/P ratio for OCP is 1.33. The OCP phase serves as the precursor of HCA, thus the precipitation of HCA is happened on OCP particles, probably. A layer of HCA can be thinner than the depth of the electron beam. So that, a proportion of electrons that are receiving to detector might be from deeper layers of OCP phase. As a result, the obtained Ca:P ratio is the ratio between 1.67 (HA/HCA) and 1.33 (OCP).

To study the phase evolution on the surface of the 6% P sample upon immersion into the SBF, the FTIR analysis is conducted. Fig. 4 displays the FTIR analysis of the 6%P sample

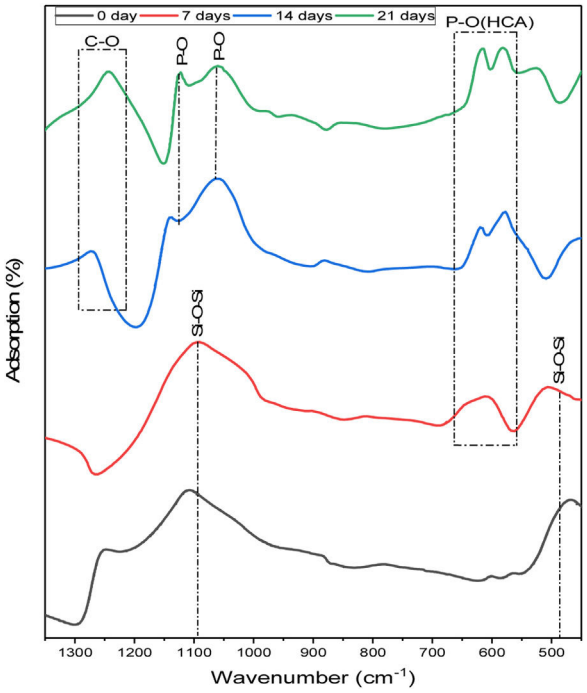

Fig. 4 – FTIR spectra of the 6%P sample immersed in SBF for different days.

immersed in SBF for 7–21 days. On day 0, two bands at approximately 1100 cm^{-1} and 465 cm^{-1} were characterized, which are associated with the asymmetric stretching vibration and bending vibration of Si—O—Si bonds, respectively [31,32]. The Si—O—Si band is evident and has not been diminished completely until 7 days. However, at 14 and 21 days this band has been deactivated and masked. On the other hand, the P—O—P band ascribed to the HCA phase starts to appear after day 7. In fact, the obtained spectra are in accordance with the synthetic HCA ones, with changes related to the intensity of the typical HCA bands, located near 1255, 1130, 1055, 605, and 560 cm^{-1} [31–34]. Also, the C—O band of HCA starts to be detected after 21 days [35].

Fig. 5 shows the MTT assay results for 6%P, 9%P, and 6%P(Ag) samples. The 9%P sample is showing higher cell viability at

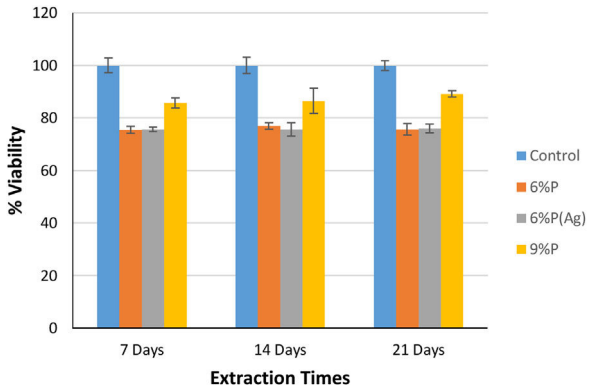

Fig. 5 – MTT assay results for 6%P, 6%P(Ag), and 9%P samples.

all times, while it showed lower bioactivity (Fig. 3). That can be justified by the evaluation of calcium ion release. The ICP results of Ca^{2+} specifies an extraordinary release from 9%P compared with 6%P (Fig. 6(a)). It is evident because of the presence of metallic calcium in the microstructure of 9%P (Fig. 2(e)); thus, it is obvious that extracted solution of this sample can bring more Ca^{2+} in contact with cells.

The morphology of MG-63 cells, immediately after seeding into culture plate and 2 h of incubation, is presented in Fig. 6(b) and (c), respectively. Moreover, the cellular morphologic response has been assessed when they are suspended into the extracted culture medium of 6%P and 9%P and seeded into culture plate and incubated for 2 h (Fig. 6(d) and (e), respectively). The outcome is the formation of cell colonies regarding 9%P samples (Fig. 6(e)), while the morphology of cells does not change by the addition of an extracted solution of

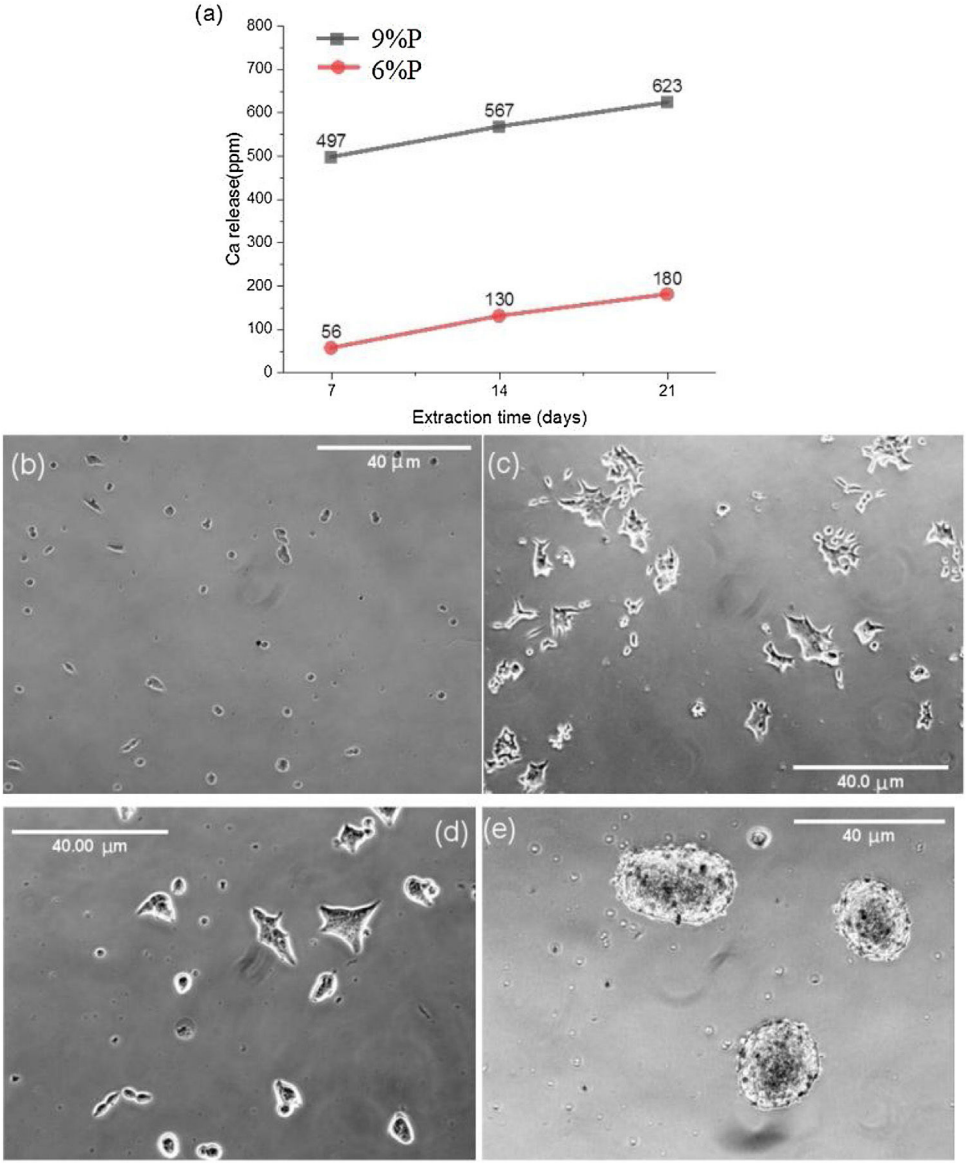

Fig. 6 – (a) Release of Ca ions from the 6%P and 9%P samples in cell culture media. The released Ca^{2+} affects the cellular morphology. The morphology of MG-63 cells as a control sample without extracted Ca^{2+} is observed (b) immediately after seeding in the culture plate, and (c) after 2 h of incubation. This morphologic response is shown when the cells are incorporated and incubated by extracted solution from (d) the 6%P sample, and (e) the 9%P sample.

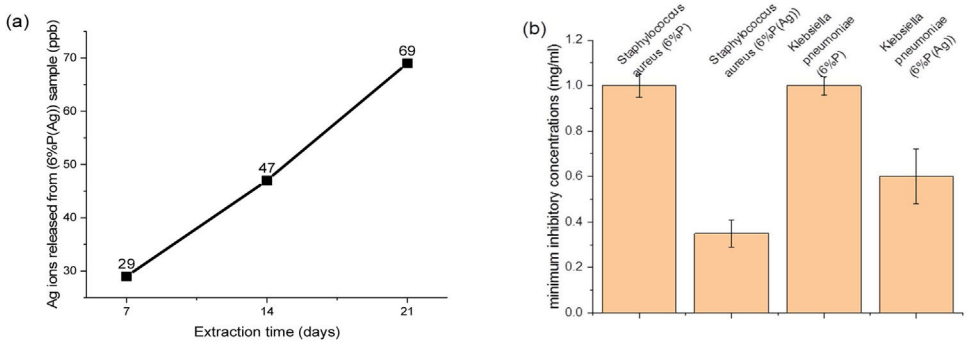

Fig. 7 – (a) The release of Ag ions from 6%P(Ag) on a ppb scale, and (b) The antibacterial effect of Ag release is evaluated as the minimum inhibitory concentration of the 6%P and 6%P(Ag) samples against Gram-negative Klebsiella pneumoniae and Gram-positive Staphylococcus aureus bacteria cells.

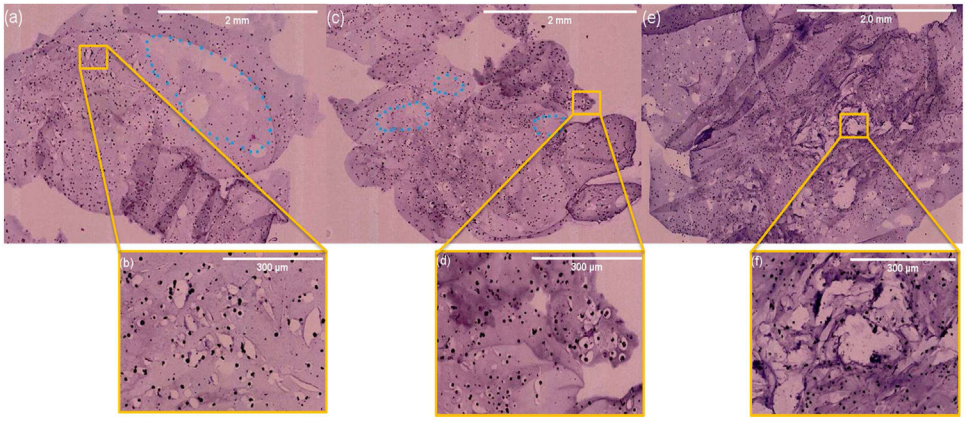

Fig. 8 – The H&E visualization of harvested scaffolds from animal models. The In vivo cell migration and attachment on the scaffolds is evident after (a, b) 5 days, (c, d) 10 days, and (e, f) 15 days.

6%P; the cells are completely wide and attached (Fig. 6(d)), similar to control plate (Fig. 6(c)). The Ca^{2+} has a crucial effect on cell-cell and cell-Protein (of natural ECM) adhesions, which are facilitated by junctions called Cadherins and Integrins, respectively [36]. In the culture plate containing MG-63 cells, the protein branches of ECM are not available, so that, the cells have two options; (1) attaching to the substrate, and/or (2) attaching to each other forming colonies. By increase of the concentration of Ca^{2+}, cells start to form cadherins among each other, so that, the cell-cell adhesion force exceeds the cell-substrate adhesion force.

Although, the effect of the extra release of Ca^{2+} by 9%P is acceptable which leads to higher viability because of attachment of cells to colonies accelerating proliferation and signaling among cells, it does not necessarily lead to osteogenesis, because the calcium ions that should be used to form HCA layers and bring osteoconduction are captured by cells forming proliferating colonies. Furthermore, it is worth mentioning that seemingly silver ions in the range of ppb (Fig. 7(a)) could not negatively affect cell growth, because as it is observed in Fig. 5, the cell viability percentage relating to sample 6%P and 6%P(Ag) are equal approximately at all time.

The main aim of incorporating Ag ions into the bioactive scaffolds is to minimize the risk of infection in injured organs through the destruction of bacterial colonies by controlled release of silver ions. Fig. 7(b) displays minimum inhibitory concentration of the 6%P and 6%P(Ag) samples against Gram-negative Klebsiella pneumoniae and Gram-positive Staphylococcus aureus bacteria cells. According to Fig. 7(b) the 6%P(Ag) scaffold showed considerable antibacterial properties against Gram-negative Klebsiella pneumoniae and Gram-positive Staphylococcus aureus bacteria cells in the presence of Ag nanoparticles. However, it showed stronger antibacterial feature against Gram-positive Staphylococcus aureus since the MIC level is lower for this bacteria cell. It is conformed that Ag nanoparticles contributes to the antibacterial properties.

In vivo evaluation of osteogenesis

After implantation of the 6%P(Ag) scaffold at the designed defects on cranium bone, the animals were kept and then sacrificed after 5, 10, and 15 days. Fig. 8 presents H&E histological results of the harvested implants. For all samples, no inflammatory cell colony was observed. According to Fig. 8(a), after 5 days the migration of cells from the adjacent sites of the native bone, and attachment on the scaffold is evident, although they are not completely distributed and infiltrated. The attachment of cells is occurred on porous and non-porous sites of the scaffold, both (Fig. 8(b)). After 10 days, more infiltration of cells is

seen, so that, cells are covering all sites of the implant (Fig. 8(c) and (d)). On the 15th day, the cells are populating in all areas (Fig. 8(e)), moreover, as it is seen in Fig. 8(f) some changes are seen in the topology of the pink background of the sample. It can be taken into account the In vivo biodegradability of the synthesized scaffold, such that, the produced holes and porosities by can be replaced by the native secreted ECM and cells. This facilitates bone repair and/or regeneration because of osteogenesis which is occurring.

Conclusions

In this study, bioactive and antibacterial silicate-phosphate porous glass-ceramic scaffolds were successfully manufactured using the PDC technique. Scaffolds possess mazelike interconnected pores of two different sizes (macro and mesopores). Scaffold contains crystalline phases like akermanite, diopside, and bioactive OCP phase. It is determined that scaffolds with a lower amount of K_2HPO_4 showed significant bioactivity. The phase evolution on the surface of the 6%P sample upon immersion into the SBF showed the formation of a complete HCA layer due to the dissolution of the OCP phase. However, MTT assay results showed higher cell viability for the 9%P sample. By morphologic evaluation of the cells in presence of extra Ca^{2+} released from the 9%P sample, it was deduced that these ions can increase cell-cell attachments forming viable cell colonies, although these colonies cannot be effective in the procedure of osteogenesis. For Ag-incorporated scaffolds, the XRD and EDS elemental analysis proved the precipitation of Ag^0 clusters. Moreover, it is confirmed that the Ag nanoparticles have a considerable role in antibacterial properties against Gram-negative Klebsiella pneumoniae and Gram-positive Staphylococcus aureus bacteria cells, as one of the main causative agents of orthopedic infections. In conclusion, the multifunctional characteristics of these scaffolds make them promising candidates for BTE applications, such that, this was assessed In vivo; not only any inflammatory cell colony was not formed on the scaffolds, but also migration and infiltration of cells across the implant was observed.

Funding

No funding is used for this work.

REFERENCES

[1] O. Faour, R. Dimitriou, C.A. Cousins, P.V. Giannoudis, The use of bone graft substitutes in large cancellous voids: any specific needs? Injury 42 (2) (2011) S87–S90, http://dx.doi.org/10.1016/j.injury.2011.06.020.
[2] S.J. Hollister, Porous scaffold design for tissue engineering, Nat. Mater. 4 (7) (2005) 518–524, http://dx.doi.org/10.1038/nmat1421.
[3] R.J. O'Keefe, J. Mao, Bone tissue engineering and regeneration: from discovery to the clinic-an overview, Tissue Eng. Part B: Rev. 17 (6) (2011) 389–392, http://dx.doi.org/10.1089/ten.teb.2011.0475.
[4] G. Turnbull, et al., 3D bioactive composite scaffolds for bone tissue engineering, Bioact. Mater. 3 (3) (2018) 278–314, http://dx.doi.org/10.1016/j.bioactmat.2017.10.001.
[5] C. Gao, et al., "Current progress in bioactive ceramic scaffolds for bone repair and regeneration, Int. J. Mol. Sci. 15 (3) (2014) 4714–4732, http://dx.doi.org/10.3390/ijms15034714.
[6] K. Whang, et al., Engineering bone regeneration with bioabsorbable scaffolds with novel microarchitecture, Tissue Eng. 5 (1) (1999) 35–51, http://dx.doi.org/10.1089/ten.1999.5.35.
[7] T. Kokubo, H.M. Kim, M. Kawashita, Novel bioactive materials with different mechanical properties, Biomaterials 24 (13) (2003) 2161–2175, http://dx.doi.org/10.1016/S0142-9612(03)00044-9.
[8] X. Chen, Y. Meng, Y. Li, N. Zhao, Investigation on bio-mineralization of melt and sol-gel derived bioactive glasses, Appl. Surf. Sci. 255 (2) (2008) 562–564, http://dx.doi.org/10.1016/j.apsusc.2008.06.101.
[9] J.R. Jones, A.R. Boccaccini, Biomedical applications: tissue engineering, in: Cellular Ceramics: Structure, Manufacturing, Properties and Applications, Wiley-VCH Verlag GmbH & Co, 2005, pp. 547–570, http://dx.doi.org/10.1002/3527606696 (Chapter 5.8).
[10] L.C. Gerhardt, A.R. Boccaccini, Bioactive glass and glass-ceramic scaffolds for bone tissue engineering, Materials 3 (7) (2010) 3867–3910, http://dx.doi.org/10.3390/ma3073867.
[11] O. Peitl Filho, G.P. LaTorre, L.L. Hench, Effect of crystallization on apatite-layer formation of bioactive glass 45S5, J. Biomed. Mater. Res. 30 (4) (1996) 509–514, http://dx.doi.org/10.1002/(SICI)1097-4636(199604)30:4<509::AID-JBM9>3.0.CO;2-T.
[12] P. Li, Q. Yang, F. Zhang, T. Kokubo, The effect of residual glassy phase in a bioactive glass-ceramic on the formation of its surface apatite layer in vitro, J. Mater. Sci. Mater. Med. 3 (6) (1992) 452–456, http://dx.doi.org/10.1007/BF00701242.
[13] M. Stevanović, N. Filipović, J. Djurdjević, M. Lukić, M. Milenković, A. Boccaccini, 45S5Bioglass®-based scaffolds coated with selenium nanoparticles or with poly(lactide-co-glycolide)/selenium particles: processing, evaluation and antibacterial activity, Colloids Surf. B Biointerfaces 132 (2015) 208–215, http://dx.doi.org/10.1016/j.colsurfb.2015.05.024.
[14] D.G. Poitout, Biomechanics and biomaterials in orthopaedics, 2nd ed., Springer-Verlag, London, 2016, pp. 1–547, http://dx.doi.org/10.1007/978-1-84882-664-9.
[15] S.S. Block, Disinfection, Sterilization, and Preservation, 5th ed., Lippincott Williams & Wilkins, 2001, pp. 1–1481.
[16] N. George, J. Faoagali, M. Muller, Silvazine® (silver sulfadiazine and chlorhexidine) activity against 200 clinical isolates, Burns 23 (6) (1997) 493–495, http://dx.doi.org/10.1016/S0305-4179(97)00047-8.
[17] A.P. Adams, E.M. Santschi, M.A. Mellencamp, Antibacterial properties of a silver chloride-coated nylon wound dressing, Vet. Surg. 28 (4) (2004) 219–225, http://dx.doi.org/10.1053/jvet.1999.0219.
[18] E.A. Deitch, A.A. Marino, V. Malakanok, J.A. Albright, Silver nylon cloth: in vitro and in vivo evaluation of antimicrobial activity, J. Trauma 27 (3) (1987) 301–304, Available: http://www.ncbi.nlm.nih.gov/pubmed/3560272.
[19] C. Vitale-Brovarone, M. Miola, C. Balagna, E. Verné, 3D-glass-ceramic scaffolds with antibacterial properties for bone grafting, Chem. Eng. J. 137 (1) (2008) 129–136, http://dx.doi.org/10.1016/j.cej.2007.07.083.
[20] C. Wu, et al., Copper-containing mesoporous bioactive glass scaffolds with multifunctional properties of angiogenesis capacity, osteostimulation and antibacterial activity, Biomaterials 34 (2) (2013) 422–433, http://dx.doi.org/10.1016/j.biomaterials.2012.09.066.

[21] G. Kaur, O.P. Pandey, K. Singh, D. Homa, B. Scott, G. Pickrell, A review of bioactive glasses: their structure, properties, fabrication and apatite formation, J. Biomed. Mater. Res. Part A 102 (1) (2014) 254–274, http://dx.doi.org/10.1002/jbm.a.34690.
[22] D. Kaur, M.S. Reddy, O.P. Pandey, In-vitro bioactivity of silicate-phosphate glasses using agriculture biomass silica, J. Mater. Sci.: Mater. Med. 31 (65) (2020) 1–13, http://dx.doi.org/10.1007/s10856-020-06402-9.
[23] H. Elsayed, P. Colombo, E. Bernardo, Direct ink writing of wollastonite-diopside glass-ceramic scaffolds from a silicone resin and engineered fillers, J. Eur. Ceram. Soc. 37 (13) (2017) 4187–4195, http://dx.doi.org/10.1016/j.jeurceramsoc.2017.05.021.
[24] P. Colombo, G. Mera, R. Riedel, G.D. Sorarù, Polymer-derived ceramics: 40 years of research and innovation in advanced ceramics, Ceram. Sci. Technol. Appl. 4 (2013) 245–320, http://dx.doi.org/10.1002/9783527631971.ch07.
[25] E. Bernardo, P. Colombo, E. Dainese, G. Lucchetta, P.F. Bariani, Novel 3D wollastonite-based scaffolds from preceramic polymers containing micro- and nano-sized reactive particles, Adv. Eng. Mater. 14 (4) (2012) 269–274, http://dx.doi.org/10.1002/adem.201100241.
[26] H. Elsayed, P. Rebesan, M.C. Crovace, E.D. Zanotto, P. Colombo, E. Bernardo, Biosilicate® scaffolds produced by 3D-printing and direct foaming using preceramic polymers, J. Am. Ceram. Soc. 102 (3) (2019) 1010–1020, http://dx.doi.org/10.1111/jace.15948.
[27] L. Fiocco, H. Elsayed, L. Ferroni, C. Gardin, B. Zavan, E. Bernardo, Bioactive wollastonite-diopside foams from preceramic polymers and reactive oxide fillers, Materials (Basel) 8 (5) (2015) 2480–2494, http://dx.doi.org/10.3390/ma8052480.
[28] A.H. Paryab, S. Abdollahi, R. Khalilifard, H.R. Madaah Hosseini, Porous slow release silicate-phosphate glasses synthesized by polymer-derived ceramics method appropriate for plants nourishment, Iran. J. Mater. Sci. Eng. 18 (1) (2021) 80–90, http://dx.doi.org/10.22068/ijmse.18.1.9.
[29] S. Abdollahi, A. Paryab, R. Khalilifard, M. Anousheh, A. Malek Khachatourian, The fabrication and characterization of bioactive Akermanite/Octacalcium phosphate glass-ceramic scaffolds produced via PDC method, Ceram. Int. 47 (5) (2021) 6653–6662, http://dx.doi.org/10.1016/j.ceramint.2020.11.003.
[30] K.C. Taşyürek, M. Buğdaycı, O. Yücel, Reduction conditions of metallic calcium from magnesium production residues, Metals (Basel) 8 (6) (2018) 383–397, http://dx.doi.org/10.3390/met8060383.
[31] J. Roman, S. Padilla, M. Vallet-Regi, Sol–gel glasses as precursors of bioactive glass ceramics, Chem. Mater. 15 (3) (2003) 798–806, http://dx.doi.org/10.1021/cm021325c.
[32] R.L. Siqueira, E.D. Zanotto, The influence of phosphorus precursors on the synthesis and bioactivity of SiO2–CaO–P2O5 sol–gel glasses and glass–ceramics, J. Mater. Sci.: Mater. Med. 24 (2) (2013) 365–379, http://dx.doi.org/10.1007/s10856-012-4797-x.
[33] D. Arcos, M. Vallet-Regí, Sol–gel silica-based biomaterials and bone tissue regeneration, Acta Biomater. 6 (8) (2010) 2874–2888, http://dx.doi.org/10.1016/j.actbio.2010.02.012.
[34] D. Bellucci, A. Sola, R. Salvatori, A. Anesi, L. Chiarini, V. Cannillo, Sol–gel derived bioactive glasses with low tendency to crystallize: Synthesis, post-sintering bioactivity and possible application for the production of porous scaffolds, Mater. Sci. Eng. C 43 (2014) 573–586, http://dx.doi.org/10.1016/j.msec.2014.07.037.
[35] R.S. Pryce, L.L. Hench, Dissolution characteristics of bioactive glasses, Key Eng. Mater. 240–242 (2003) 201–204, http://dx.doi.org/10.4028/www.scientific.net/kem.240-242.201.
[36] R.I. Freshney, Culture of Animal Cells: A Manual of Basic Technique and Specialized Applications, John Wiley & Sons, 2015.